Supplementary Information

C. Guerrier[1], J.A. Hayes[2], G. Fortin[2], D. Holcman[1]

This SI is divided into 3 parts. In the first part, we complement the experimental procedure, providing details about short-term depression analysis in the preBötzinger Complex, and we provide specific information about the modeling aspect. We describe the dynamics of the membrane potential, synaptic facilitation and the two step synaptic depression model. We further describe synaptic connections between neurons. In the second part, we present additional simulations. The third part describes the legends for the movies mentioned in the main text.

1 Complement on the Material and Methods

1.1 Experimental procedure

Swiss mice (P0-P4) were anesthetized and dissected in artificial cerebrospinal fluid (ACSF) containing (in mM): 132.5 NaCl, 8 KCl, 0.58 Na_2HPO_4, 8.5 $NaHCO_3$, 30 D-glucose, 1.26 $CaCl_2$, 1.15 $MgCl_2$. Hindbrains were quickly removed and embedded within a 4% agarose block and glued to the pedestal of a Leica microtome. Transverse slices were cut from the medulla (450 μm thick) where the rostral surface was 400-500 μm caudal to the caudal end of the facial nucleus in line with the calibrated atlas of [1]. Slices were then placed into a recording chamber and held down by a platinum grid with nylon fibers. The slices were perfused with $30-31\,^{\circ}$C extracellular ACSF for at least 30 min before patch recording commenced.

Tissue was visualized using a Nikon Eclipse upright microscope in IR-DIC configuration using a water-immersible 40x objective and a CoolSnap HQ2 camera (Photometrics, AZ) controlled by Micro-Manager [2]. Whole-cell patch recordings were performed with a MultiClamp 700B, digitized by a 1440a Digidata, and controlled by pClamp 10 (Molecular Devices, CA). The intracellular patch solution contained (in mM): 123 K-gluconate, 21 KCl, 0.5 EGTA, 10 HEPES, 3 $MgCl_2$. Picrotoxin (5 μM) and strychnine (5 μM) were bath-applied to block $GABA_A$ and glycinergic synaptic currents.

Evoked excitatory postsynaptic currents (eEPSCs) were identified by patch-recording preBötC respiratory neurons and electrically stimulating the midline of the slice just dorsal to the midline aspect of the inferior olive (Fig. 3A-B) using an ISO-Flex stimulation isolation unit (A.M.P.I., Israel). Once a respiratory neuron was identified, the bath $[K^+]$ was dropped to 3 mM to reduce spontaneous respiratory activity. Low-intensity electrical pulses were applied for 100 μs duration approximately every 9 s and the intensity increased until >50% of the pulses resulted in eEPSCs observed in the voltage-clamp recording. After that, we switched to gap-free recording and periodically stimulated trains of variable length and frequency to investigate the postsynaptic response. The eEPSCs were identified and quantified offline using *PhysImage* software

[1]Group of Applied Mathematics and Computational Biology, Ecole Normale Supérieure, 46 rue d'Ulm 75005 Paris, France.

[2]Université Paris-Saclay, Université Paris-Sud, CNRS, UMR 9197, Institut des Neurosciences Paris-Saclay, F-91190, Gif-sur-Yvette, France.

(http://physimage.sourceforge.net/).

1.2 Hodgkin-Huxley Model of the membrane potential

To model the membrane potential of each neuron, we used a simplified Hodgkin-Huxley model, where we considered the changes in Na^+, K^+ and leak channels. We further added the synaptic currents generated from connected neurons. The resting potential of each neuron was at a mean of -65.1 mV, distributed randomly according to a Gaussian distribution with variance 0.2. To account for the spontaneous fluctuations of the membrane potential, we added a Gaussian noise source term to the potential with a variance σ. The equations are

$$C\dot{V} = I_{app} - I_{Na} - I_K - I_L + \sum_j I_{syn,j} + \sigma\dot{W} \quad (1)$$

$$\dot{n} = \alpha_n(1-n) - \beta_n n \quad (2)$$

where

$$\begin{aligned} I_{Na} &= g_{Na} m_\infty^3 h(V - E_{Na}) \\ I_K &= g_k n^4 (V - E_K) \\ I_L &= g_L(V - E_L) \\ m_\infty &= \frac{\alpha_m}{\alpha_m + \beta_m} \\ \alpha_k &= \frac{1}{\tau_k} \frac{\theta_k - V}{e^{\frac{\theta_k - V}{\tau_k}} - 1} \text{ for } k = n, m \\ \beta_k &= \eta_k e^{-\frac{V+65}{\sigma_k}} \end{aligned}$$

The variables m and n represent the opening of the Na^+ and K^+ channels respectively. We used the following approximation for the closing of the Na^+ channel $h = (0.89 - 1.1n)$. The synaptic current $\sum_j I_{syn,j}$ integrates the sum over all connecting neurons that we shall describe next. The term $\dot{W}$ in eq. 1 represents the derivative of standard white noise. Indeed, in the discretized form, $W(t+\Delta t) - W(t) = \sqrt{\Delta t} Z$ where Z is a Gaussian variable of mean 0 and variance 1.

1.3 Model of the synaptic dynamics

To characterize the synaptic dynamics, we built a two pool model that accounted for two different time scales of depression. Indeed, synaptic depression results from the depletion of the readily releasable pool (RRP) (Fig. 1A), where synaptic vesicles are gathered at the membrane before fusion. We also accounted for the other pool of recycling vesicles (recycling pool, RP) that are diffusing. Finally after fusion, vesicles are not participating in any of the two previous pools. This state is described as recovering. In the present model, we considered that the total amount

of vesicles at a synapse is constant. Thus the fraction $y_{\rm free}$ (resp. $y_{\rm dock}$) of vesicles in the RP (resp. RRP), with the fraction of recovering vesicles $y_{\rm rec}$ satisfies the conservation equation

$$y_{\rm free} + y_{\rm dock} + y_{\rm rec} = 1. \tag{3}$$

Finally, the synaptic facilitation variable x reflects all possible mechanisms that enhance vesicular release, and thus is associated with an increase in the release probability [3]. It is given by

$$\dot{x} = \frac{X - x}{\tau_f} + k(1 - x)H(V - T), \tag{4}$$

where τ_f is the facilitation rate, X its value at equilibrium, and H is the Heaviside function. The facilitation x increases due to the term $k(1-x)$ during an Action Potential (AP), when the membrane potential V is above a threshold T ($H(V-T)=1$), and relaxes back to equilibrium when V is below T ($H(V-T)=0$).

We shall now present the mass action equations that describe the vesicular exchanges between different pools. The amount of vesicles in the RP depends on the arrival of vesicles from the recovering state, given by the flux $\Phi_{\to \rm RP} = \dfrac{y_{\rm rec}}{\tau_{\rm rec}}$, where $\tau_{\rm rec}$ is the delivery time. The outward flux of vesicles is proportional with the rate constant $\tau_{\rm dock}$ to the fraction of available sites $(y^{\rm max}_{\rm dock} - y_{\rm dock})$ at RRP, where $y^{\rm max}_{\rm dock}$ is the maximal number of sites in the RRP, and to the fraction of available vesicles in the RP. Finally, the outward $\Phi_{\to \rm RRP}$ is generated in the absence of an AP by the intrinsic turn over, when the membrane potential is below a threshold T. However, when the membrane potential is above the threshold T, $\Phi_{\to \rm RRP}$ depends on the facilitation variable x and we finally get

$$\Phi_{\to \rm RRP} = \frac{1}{\tau_{\rm dock}} \left(y^{\rm max}_{\rm dock} - y_{\rm dock}\right) y_{\rm free} \left[1 + \frac{x - X}{X} H(V - T)\right]. \tag{5}$$

Finally,

$$\begin{aligned} \dot{y}_{\rm free} &= \Phi_{\to \rm RP} - \Phi_{\to \rm RRP} \\ &= \frac{y_{\rm rec}}{\tau_{\rm rec}} - \frac{1}{\tau_{\rm dock}} \left(y^{\rm max}_{\rm dock} - y_{\rm dock}\right) y_{\rm free} \left[1 + \frac{x - X}{X} H(V - T)\right]. \end{aligned} \tag{6}$$

The equation for the fraction $y_{\rm dock}$ of vesicles in the RRP is given by the balances of inward vesicles arriving from the RP, $\Phi_{\to \rm RRP}$ (eq. 5), and on the flux of released vesicles $\Phi_{\rm RRP \to}$, which vanishes in the absence of an AP. Following a stimulation, it is proportional to the fraction $y_{\rm dock}$ of vesicles in the RRP and to the facilitation variable x with a rate $\tau_{\rm rel}$:

$$\Phi_{\rm RRP \to} = \frac{1}{\tau_{\rm rel}} y_{\rm dock} \left(\frac{x - X}{X}\right) H(V - T). \tag{7}$$

Balancing the fluxes $\Phi_{\to \rm RRP} - \Phi_{\rm RRP \to}$ leads to

$$\begin{aligned} \dot{y}_{\rm dock} &= \frac{1}{\tau_{\rm dock}} \left(y^{\rm max}_{\rm dock} - y_{\rm dock}\right) y_{\rm free} \left[1 + \frac{x - X}{X} H(V - T)\right] \\ &\quad - \frac{1}{\tau_{\rm rel}} y_{\rm dock} \frac{x - X}{X} H(V - T). \end{aligned} \tag{8}$$

Finally, changes in the amount of recovering vesicles $y_{\rm rec}$ is equal to the difference of the fluxes $\Phi_{\to \rm RRP}$ and $\Phi_{\to \rm RP}$, which leads to

$$\dot{y}_{\rm rec} = \Phi_{\rm RRP\to} - \Phi_{\to \rm RP} = \frac{1}{\tau_{\rm rel}} y_{\rm dock} \frac{x - X}{X} H(V - T) - \frac{y_{\rm rec}}{\tau_{\rm rec}}. \tag{9}$$

In summary, using the conservation equation 3, we obtain the following system of equations

$$\begin{aligned}
\dot{x} &= \frac{X - x}{\tau_f} + k(1 - x)H(V - T) \\
\dot{y}_{\rm free} &= \frac{1 - y_{\rm free} - y_{\rm dock}}{\tau_{\rm rec}} - \frac{1}{\tau_{\rm dock}} \left(y_{\rm dock}^{\rm max} - y_{\rm dock}\right) y_{\rm free} \left[1 + \frac{x - X}{X} H(V - T)\right] \\
\dot{y}_{\rm dock} &= \frac{1}{\tau_{\rm dock}} \left(y_{\rm dock}^{\rm max} - y_{\rm dock}\right) y_{\rm free} \left[1 + \frac{x - X}{X} H(V - T)\right] \\
&\quad - \frac{1}{\tau_{\rm rel}} y_{\rm dock} \frac{x - X}{X} H(V - T).
\end{aligned} \tag{10}$$

1.4 Computing the synaptic current I_{syn}

To compute the synaptic current between two connected neurons, we used the synaptic model described above. The postsynaptic current $i(t)$, due to an action potential generated in the presynaptic neuron is proportional to the amount of released vesicles $(y_{\rm dock}(t) - y_{\rm dock}(t_0))$, where t_0 is the time of the presynaptic AP. It is set to zero when the RRP is empty.

To account for the inherent discrepancy between the continuous description of the fraction of vesicles in the RRP and the actual discrete number, we imposed an empty RRP when the variable $y_{\rm dock}$ was below $y_{\rm dock}^{\rm min} = 0.04$. This minimal value for $y_{\rm dock}$ corresponds to a total of around twenty-five vesicles in the synapse and to a mean maximal number of vesicles in the RRP of 4.5. The threshold $y_{\rm dock}^{\rm min}$ was chosen by plotting the variable $y_{\rm dock}$ during a protocol where the membrane potential V was constantly stimulated at 60 Hz for 2 seconds, which reflects the mean spike frequency during bursting. The variable $y_{\rm dock}$ decreased abruptly during the first 500 ms, and then slowed down before reaching an asymptotic regime. From these considerations, we chose the value of threshold $y_{\rm dock}^{\rm min}$ in the intermediate regime, before $y_{\rm dock}$ enters its asymptotic regime (Fig. S1**F**, the red line shows the asymptotic regime, when the tangent of $y_{\rm dock}(t)$ is equal to the limit value of the one at infinity, computed by a numerical fit).

After a bursting event, we implemented a refractory period (RefP) reflecting that in order for the synapse to recover and for a vesicle to be released, several vesicles need to accumulate at the active zone. This refractory period is monitored using the facilitation variable x, and ends when it reaches the value $x_{\rm RefP} = 0.31$, close to its equilibrium value $X = 0.3$ (eq. 4).
Finally, when a presynaptic AP arrived at a time t_0, which does not fall into the refractory period window, the synaptic current is

$$i_{t_0}(t) = K_I(y_{\rm dock}(t) - y_{\rm dock}(t_0))H(V - T)H\left(y_{\rm dock} - y_{\rm dock}^{\rm min}\right), \tag{11}$$

where K_I is a constant, which converts the proportion of fused vesicles during an AP, into a postsynaptic current. For spikes arriving at times t_k, the synaptic current is for $t \in [t_k, t_{k+1}]$,

$$I_{syn}(t) = \begin{cases} 0 \text{ during a refractory period} \\ i_{t_k}(t - \tau_{\text{del}}), \text{ else} \end{cases} \tag{12}$$

where $\tau_{\text{del}} = 1$ ms is a delay.

1.5 Constructing the network connectivity

We present now the connectivity map for the network that we implemented between neurons. Neurons were distributed on a square lattice (Fig. 1B) and were connected randomly according to the probability distribution

$$\mathbf{P}(i \to j) = \exp(-d(i,j)^2/(2s^2)) \tag{13}$$

for neuron i and j and the parameter s, that is specified later on, and where $d(i,j)$ is the Euclidian distance between neurons i and j normalized by the minimal distance between two neurons. For $s = 0.9$, the mean number of output connections per neurons was around 3.7, and the mean total number of connections was around 7.5.

As presented in Fig. S2, the probability to connect directly to one of the 8 proximal neighbors was around 0.3, whilst for the second square it dropped to 0.1. More than 99 % of the network (around 396 neurons out of 400) were part of the network. Thus only few neurons were completely isolated.

1.6 Summary of the network dynamics

For a neuronal network consisting of 20 x 20 (i.e. 400) neurons organized on a square lattice, we modeled the synaptic properties and voltage as previously described. We studied various network configurations (for various s) and also studied the effect of changing the size. However, during each simulation, the connections will be kept fixed. In summary, each neuron is then described by four differential equations (one for the action potential and three for the synaptic dynamics, Fig. S1, see also movies S1-S2-S3)

$$\begin{aligned}
C\,\dot{V}_i &= -I_{Na} - I_K - I_L + \sum_{j \text{ connected to } i} I_{syn,j} + \sigma \dot{W} \\
\dot{x}_i &= \frac{X - x_i}{\tau_f} + k(1 - x_i) H(V - T) \\
\dot{y}_{\text{free},i} &= \frac{1 - y_{\text{free},i} - y_{\text{dock},i}}{\tau_{\text{rec}}} - \frac{1}{\tau_{\text{dock}}} \left(y_{\text{dock}}^{\max} - y_{\text{dock},i}\right) y_{\text{free},i} \left[1 + \frac{x_i - X}{X} H(V - T)\right] \\
\dot{y}_{\text{dock},i} &= \frac{1}{\tau_{\text{dock}}} \left(y_{\text{dock}}^{\max} - y_{\text{dock},i}\right) y_{\text{free},i} \left[1 + \frac{x_i - X}{X} H(V - T)\right] \\
&\quad - \frac{1}{\tau_{\text{rel}}} y_{\text{dock},i} \frac{x_i - X}{X} H(V - T),
\end{aligned} \tag{14}$$

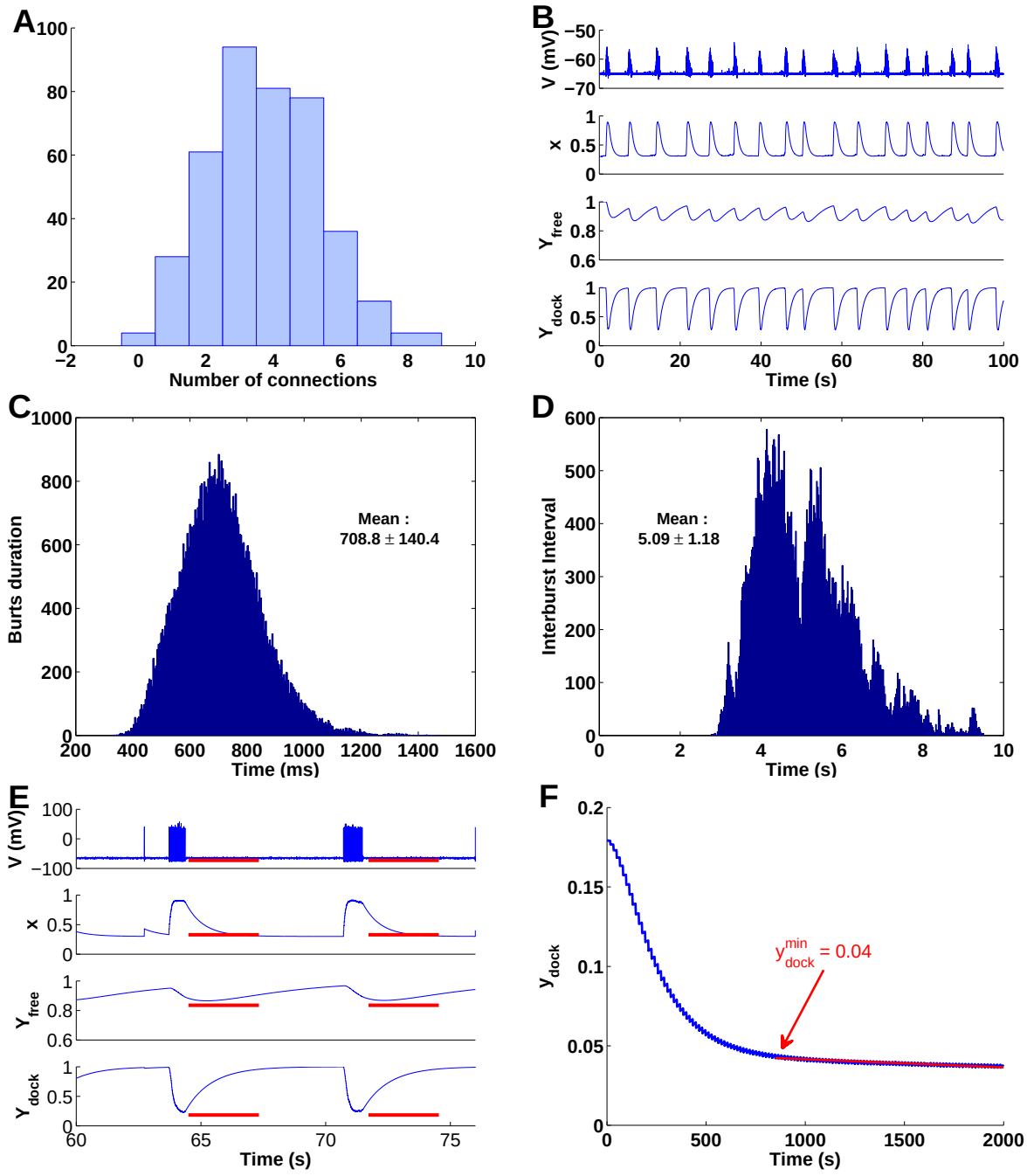

Figure S1: **Histogram of the number of output connections per neuron, and network rhythmic activity with 400 neurons**. **A**: Histogram of the number of output connections per neuron associated to Fig. 1B. Here, the mean number of output connections is 3.75. **B**: Mean voltage V, depression and facilitation average over the network. **C**: Bursting duration histogram (average over one network monitored during 900 sec): the mean burst duration is 708 ± 140 ms. **D**: Interburst interval histogram (mean : 5.1 ± 1.2 sec). The histogram of the interburst interval displays two different peaks at T=4.3 sec and T=5.4 sec, which shows that the rhythm is multimodal. **E**: Zoom on the voltage V, the facilitation variable x and the two scaled depression variable $Y_{\text{free}} = y_{\text{free}}/y_{\text{free}}^{\max}$ and $Y_{\text{dock}} = y_{\text{dock}}/y_{\text{dock}}^{\max}$ for a single neuron during sixteen seconds. The red bars represent the refractory period coming after a burst. **F**: Dynamics of the depression variable y_{dock} during a 60 Hz stimulation lasting two seconds. The red line shows the asymptotic regime.

where $i = 1..400$. All the simulations are performed in MATLAB (Mathworks, MA), using the RK4-ode solver with a step time $\Delta t = 0.05$ ms, and with the set of parameters described in Table 1. Results are expressed as mean ± S.E.M. MATLAB code for this model is accessible on the authors' website (http://www.bionewmetrics.org).

2 Complementary simulations

2.1 Decreasing the network connectivity gradually suppresses the endogenous rhythm. Fig. S2

To study the influence of scaling synaptic connections, we decreased the value of the connectivity parameter s from 0.9 (initial network) to 0.7, (connection probability, see eq. 13 and Fig. S2A), while keeping the neuronal resting membrane potentials at the same values. We first investigated how the connecting probability was decreased for increased distances between neurons (Fig. S2B). Each block represents the probability to connect neighboring neurons: the first four closest are on bar 1 and so on (see details on Fig. S2B). In summary, as long as $s \geq 0.85$ (mean number of output connections $M_{CN} = 3.2$) the network dynamics is not much affected (Fig. S2C-D-E). However, lowering s below 0.75 leads to $M_{CN} = 2.3$, the bursting pattern remains, but the interburst intervals show a large variability, lasting in some cases 25 sec instead of 5 sec. For $s < 0.7$, ($M_{CN} = 1.9$), the rhythm disappears, the network can generate bursts between silent periods that can last more than 100 seconds. This result is confirmed by the power spectrum analysis (Fig. S2D). We conclude here that a minimal network connectivity is required to induce periodic bursting patterns.

The neuronal connectivity characterized here by the variable s is the key parameter governing the network rhythm. We could discern three different regimes depending on the value of s: for $s < 0.8$, the network expresses irregular bursting patterns, due to a high variability in the interburst interval duration. In that case, the mean number of connections per neurons (M_{CN}) is below 3. This small amount of connections prevents the propagation of Action Potentials (APs) within the network, preventing the recruitment of neurons required for burst induction (Supp Movie S6). When the connectivity parameter s is in the range $0.8-1$, M_{CN} varies approximatively between 3 and 5. The network expresses regular bursting patterns, and APs propagate quickly within the whole network (Supp Movie S3). Finally, when the parameter $s > 1$, the $M_{CN} > 5$, and network bursts cannot terminate (Fig. S2F). Interestingly, during these periods, the RRP never empties (Fig. S2F). This results from the low spiking frequency (around 20 Hz) during bursting, which permits a steady-state refilling of vesicles. This low frequency results from the high efficient propagation of AP in the network, as illustrated in Movie S7. Indeed, an AP can generate a wave of APs that crosses the entire network very quickly, followed by another wave of depolarization, which prevents the recurrent excitation observed in Movie S3. Thus a high connectivity between neurons leads to waves of APs in the networks, as studied in [4].

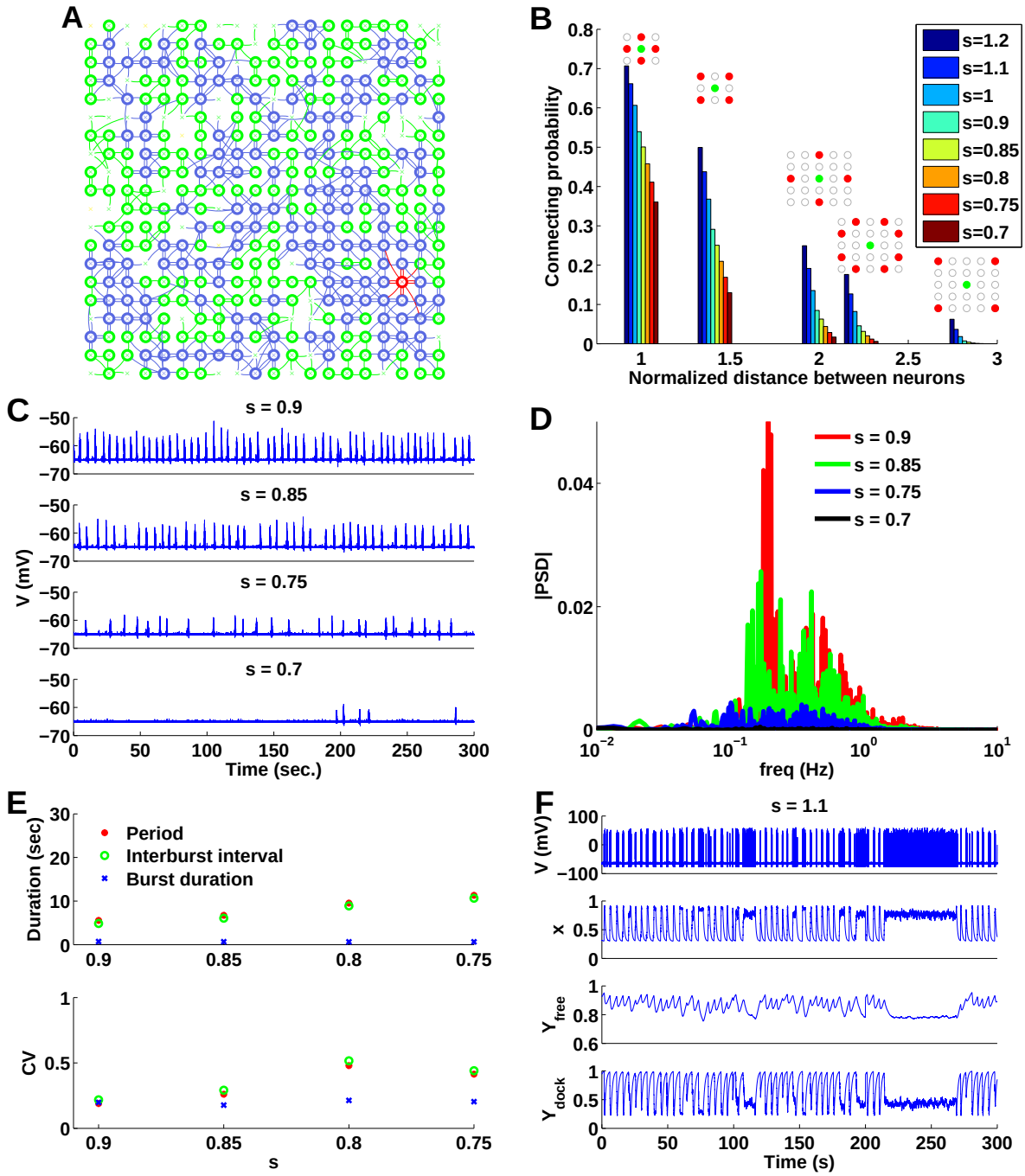

Figure S2: **Effect of connectivity on the network rhythm A**: Example of a network (400 neurons) connected with parameter $s = 0.75$ (Materials and Methods). **B**: Empirical distribution of neuronal connections. **C**: Mean membrane potential for networks generated with $s = 0.9, 0.85, 0.75$ and 0.7, where the mean number of output connections per neuron (M_{CN}) is 3.8, 3.2, 2.3 and 1.9 respectively. **D**: Power spectrum of the mean membrane potential computed for the entire network. **E**: Mean and CV of the burst duration, interburst interval and the period as a function of s. **F**: Time dependent plot of the voltage and the scaled variables Y_{free}, Y_{dock} and $\boldsymbol{x}$ for a single neuron chosen randomly from the network in the case of a very high network connectivity, when $s = 1.1$ ($M_{CN} = 6$).

2.2 Histograms of the interburst interval for four different network realizations. Fig. S3

Neuronal network dynamics can also be characterized by the interburst interval. Indeed, different network realizations with identical synaptic and electrophysiological parameters lead to different interburst interval distributions, while the mean is identical (Fig. S3).

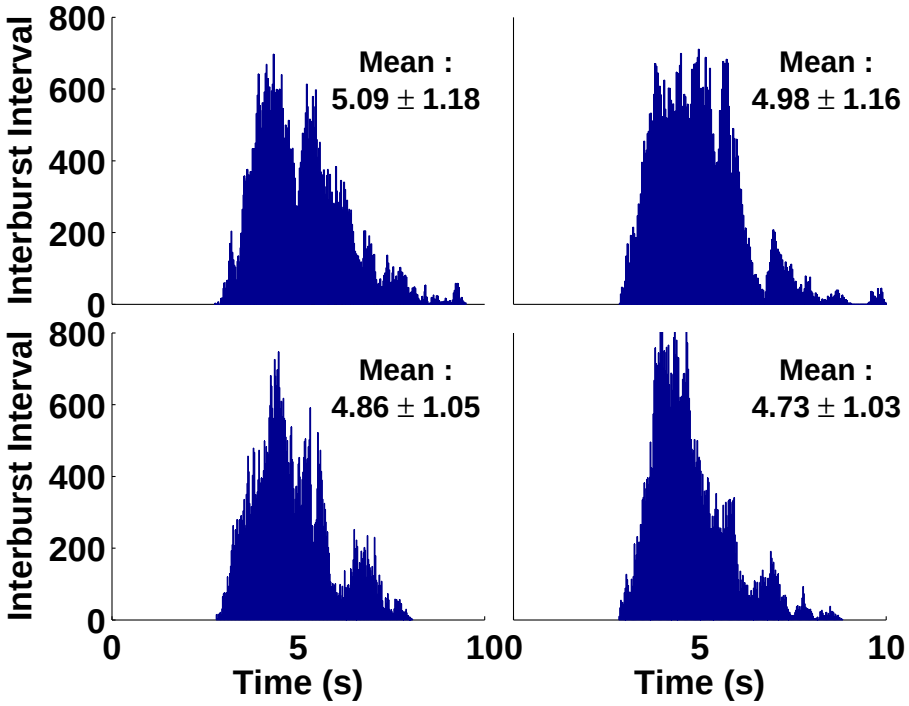

Figure S3: **Histograms of the interburst interval for four different network realizations, generated with identical synaptic and electrophysiological parameters (400 neurons)**. The networks have different neuronal organization. The histograms show several peaks, at different times: top-left) Tpeaks=4.3 and 5.4 sec. top-right) Tpeaks=3.8, 4.5, 4.9 and 5.7 sec. bottom-left) Tpeaks=4.3, 5.2 and 5.6 sec. bottom-right) Tpeaks=4.0 and 4.4 sec.

2.3 Influence of the synaptic properties on the network. Fig. S4-S5

To explore the parameter space in our model, we studied the influence of four key synaptic parameters on the network rhythm: the facilitation time constant τ_f, the vesicular fusion time τ_{rel}, the docking time τ_{dock} and the recovery time τ_{rec} (the synaptic dynamics is summarized in the system of eqs. 10 and the associated parameters are reported in Table 1). Using a neuronal network containing 400 neurons, we ran simulations similar to Fig. 1D and the results are shown in Fig. S4. We evaluated how the rhythm was altered when changing the four parameters (time

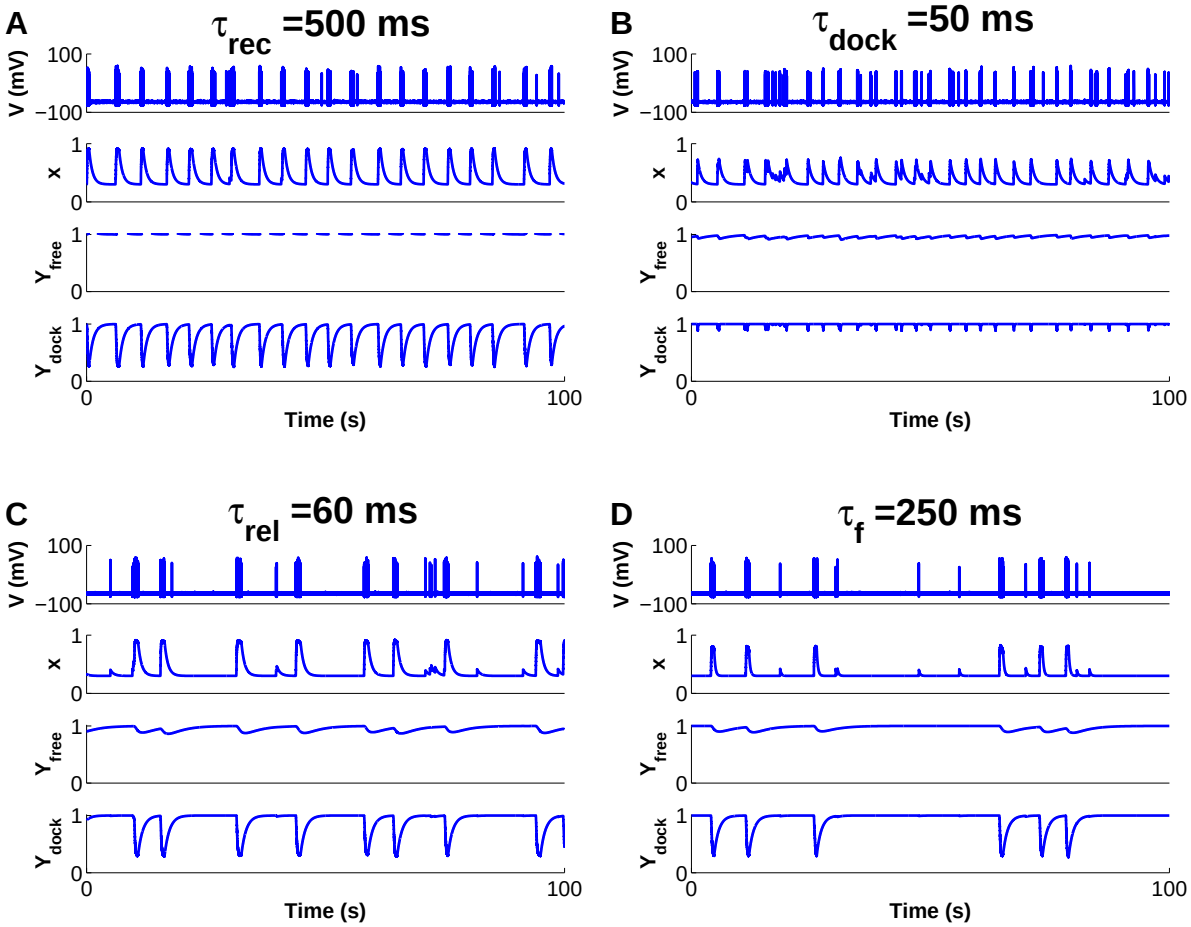

Figure S4: **Responses of the network and mean synaptic properties.** We have shown below the neuronal response, the graph for x (facilitation), Y_{free} (depression 1), Y_{dock} (depression 2). We changed the parameter written on top of each sub-figure. The rest of the parameters are the ones in Table 1.

scales) described above and ran simulations for 100 sec, and varied the different time scales (one at a time) while fixing the others. The results are shown in figure Fig. S5.

The time constant for vesicular recovery τ_{rec} has almost no influence on the cycle period and the burst duration (Fig. S5**A**). The influence of the time scale for switching from the RP to RRP (τ_{dock}) is also almost negligible, but decreasing τ_{dock} to a value of 50 ms leads to a network desynchronization (Fig. S4**B** and Fig. S5**B**) and disruption of the rhythm.

Increasing the time constant for the vesicular depletion in the RRP (τ_{rel}) from 10 ms to 60

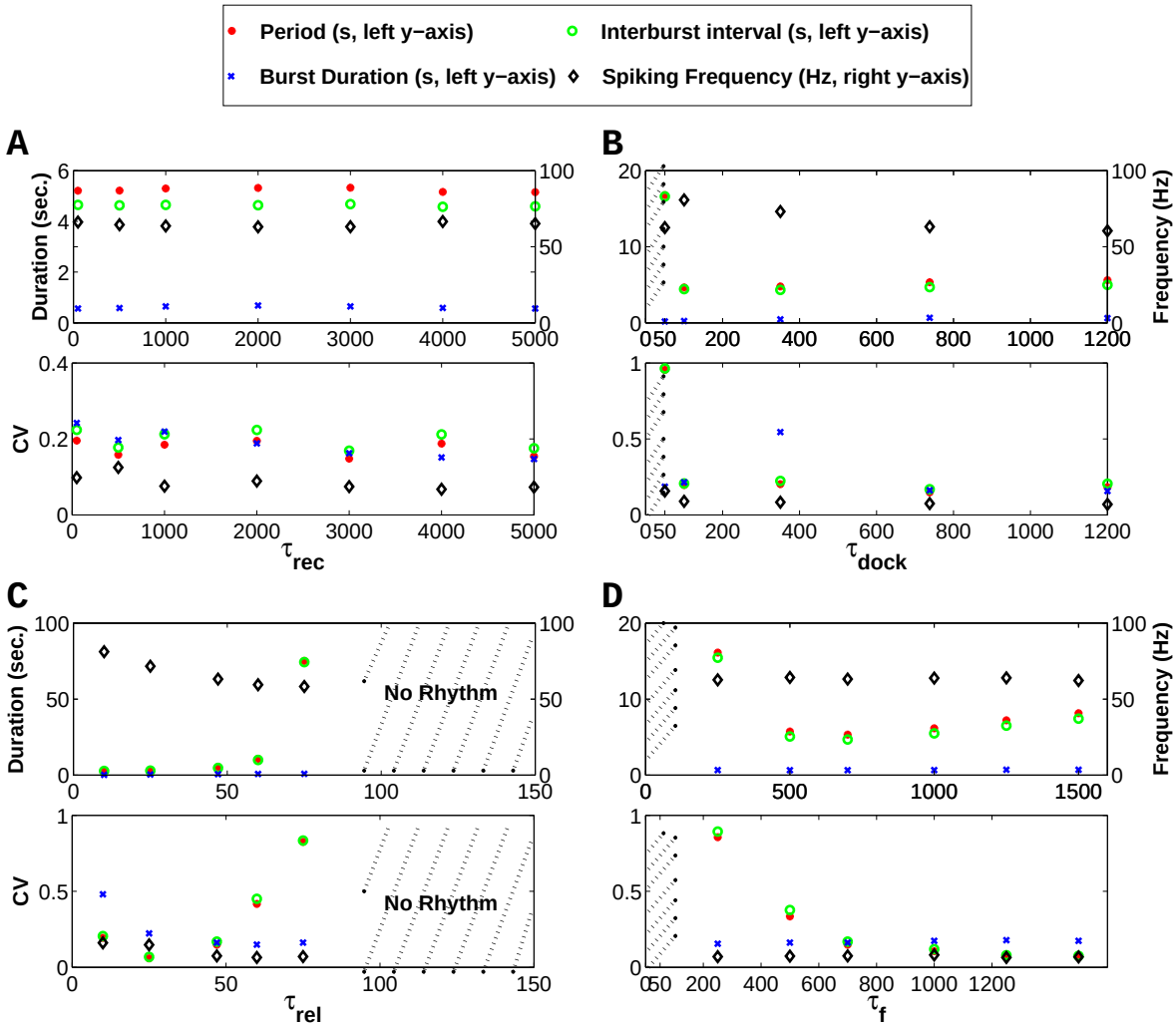

Figure S5: **Synaptic dynamics at the network level:** Mean and CV of the burst duration, the interburst interval, the cycle period (left y-axis, sec), and the spiking frequency during bursts (right y-axis, Hz) as a function of $\tau_{\rm rec}$ (**A**), $\tau_{\rm dock}$ (**B**), $\tau_{\rm rel}$ (**C**) and τ_f (**D**). All the other parameters are the same as described in Table 1, except $y^{\rm min}_{\rm dock}$ (eq.10 of SI), which is computed for each value of τ_x. The network is the same for each simulation.

ms widely increases the cycle periods from 2.9 ± 0.6 sec to 10.7 ± 0.1 sec, and also the burst duration from 200 ± 100 ms to 772 ± 115 ms. In addition, past the value $\tau_{\text{rel}} = 75$ ms, the rhythm is unstable, with cycle periods of 75.1 ± 61.9 sec, and burst duration of 851 ± 138 ms (Fig. S4**C**).

Finally, by increasing the time constant for the facilitation variable (τ_f), the cycle period increases linearly. More interestingly, decreasing τ_f from 700 ms to 250 ms widely increases the cycle period and variability from 5.3 ± 0.8 sec to 16.1 ± 13.8 sec respectively. This increase is due to the difficulty in recruiting neighboring neurons, as the facilitation variable $x(t)$ drops to its steady state too quickly. However, the burst duration is stable, changing from 650 ± 100 ms to 666 ± 100 ms.

Technically, when we modified these four time constants, the dynamics of Y_{dock} ($Y_{\text{dock}} = \frac{Y_{\text{dock}}}{y_{\text{dock}}^{\max}}$) are changed and we had to modify the value of $y_{\text{dock}}^{\min}$ accordingly. Indeed, the value of $y_{\text{dock}}^{\min}$ is chosen to represent the value of Y_{dock} that accounts for the emptiness of the RRP. This parameter is key in the transformation from the continuous model and the discrete number of vesicles (see Supplementary Information section "Computing the synaptic current"). To choose $y_{\text{dock}}^{\min}$ for the previous set of parameters (Table 1), we applied a 60 Hz stimulation protocol to a single neuron, and chose for termination of release the first time for which the derivative of $Y_{\text{dock}}(t)$ is equal to the limit value of the tangent at infinity, computed by a numerical fit. We applied the same procedure for each of the four time-related parameters. We then ran simulations for each value during 300 sec while keeping the same neuronal network. For $\tau_f = 50$ ms, 100 ms, 250 ms and $\tau_{\text{rel}} = 75$ ms, 100 ms, the cycle period was above 10 sec, and we ran longer simulations for about 1500 sec to obtain enough cycles.

2.4 Modification of the spiking frequency during a burst. Fig. S6

The mean spiking frequency during bursts is around 60 Hz, and is stable under the different conditions we imposed to the model. This frequency was not fixed, but emerged as a results of the simulations with the parameters of the model described in Table 1. To determine which parameters could control this frequency, we decreased the re-polarization constants α_n and β_n in equation 2, that govern potassium dynamics in the HH model. This results in slowing down the dynamic of the variable n, which increases the refractory period of the AP. It also reduces the minimal current I_{app} needed to induce an AP. To compare the dynamics of the model for different values of α_n and β_n, we also modify the amplitude of the voltage noise σ and the synaptic strength K_I: when parameters α_n and β_n are scaled by a factor 0.35 in eq. 2, the AP-threshold in the HH dynamic reduces from -21.6 mV to -28.4 mV. After we further reduce the amplitude of the noise σ eq. 1 from 0.4 to 0.2, and the synaptic strength K_I (eq. 11) from 2666 to 2250, we simulated the bursting activity of the network and the results are presented in Fig. S6, which affect the network dynamics as follows:
-the spiking frequency is decreased during a burst, from 59 Hz to 34.8 ± 10 Hz,
-the mean number of spikes within a burst is decreased from 42 to 10.4,
-the burst duration is decreased from 694 ± 138 ms to 315 ± 225 ms,
-the cycle period has decreased from 5.5 ± 1 sec to 3.4 ± 1.7 sec.

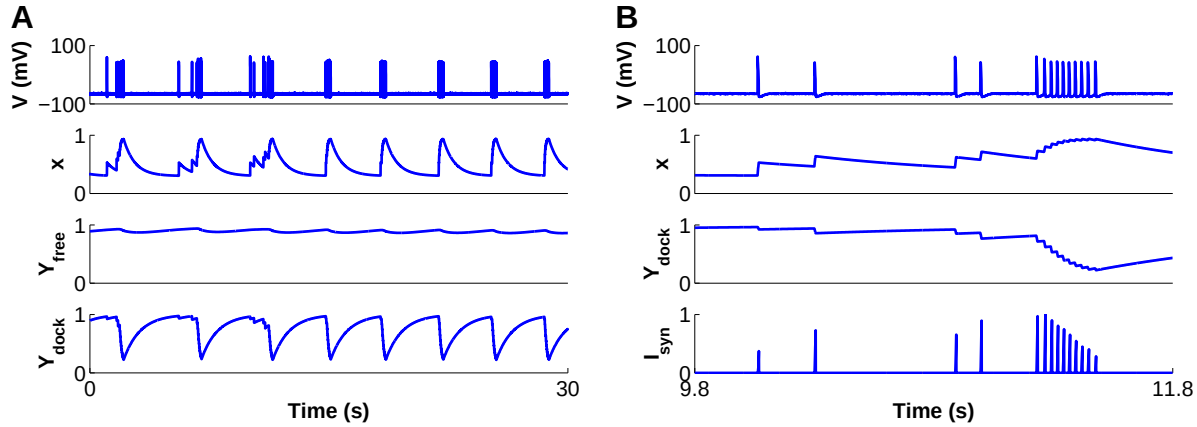

Figure S6: **Burst Spiking Frequency A**: Time dependent plot of the voltage V, the facilitation variable x, and the scaled variables Y_{free}, Y_{dock} for a single neuron chosen randomly from the network for a scaling of variables α_n and β_n of 0.35, with parameter $\sigma = 0.2$ and $K_I = 2252$ (the mean bursting duration is 315 ± 225 ms, and the mean cycle period is 3.4 ± 1.7 s). **B**: Magnification of V, x, Y_{dock} and I_{syn} for the neuron of Fig. S6A, during 1.5 s

2.5 Effect of deleting random neurons on the network activity. Fig. S7

We randomly suppressed different neurons (from 25 to 200 in a network of 400 neurons) by removing their connections with the rest of the network. We ran, for each number of removed neurons, three simulations for 100 sec. and for different random network realizations. We found that the rhythm was not changed by adding more simulations. However the rhythm period kept increasing when deleting more neurons. When at least 125 neurons are suppressed, the rhythm period exceeds 15 seconds, and thus we increased the time window of simulation to 300 seconds to observe many cycles. When removing 175 neurons, the number of bursts decreased drastically, leading to quiet periods lasting more than 300 seconds, and to rhythm disruption.

We compare in Fig. S7 the rhythm period obtained by suppressing an increasing number of neurons in the simulations, with lesioning by cumulative single-cell laser ablation (Fig. 5c in [5]). Interestingly, we could fit both the experimental and simulation data with a single exponential curve (Fig. S7A), although we found that a double exponential is a better approximation (dashed curve in Fig. S7A). The goodness of fit as measured by the summed square of residuals (SSE) = 0.002. To compare the bursting period, we first normalized by the one obtained in the absence of any neuronal removal. Since the number of removed neurons to rhythm disruption was not known, we used our numerical simulations to estimate this number. We found that the rhythm was completely abolished between 150 and 175 neurons removed, and fixed 160 for a complete rhythm disruption (Fig. S7A). We represent the average time-dependent voltage changes over the neuronal population (Fig. S7B) and the associated power spectrum density (PSD) absolute value (Fig. S7C).

When no neurons are removed, (Fig. S7C, red, x-axis is in logarithmic scale) the absolute value of the PSD presents a main peak around f_0 =0.2 Hz (fundamental frequency), followed by several peaks at different frequencies that are integer multiples of f_0 and represents the harmonics. This analysis shows that our system is almost periodic, with a mean frequency around 0.2 Hz.When 50 neurons are removed (12.5 % of the network), the network activity is not seriously damaged; with 100 neurons (25 % of the network), the rhythm starts to be affected and it disappears by removing 175 neurons and more. The mean burst duration (interburst intervals, periods) are plotted in Fig. S7D. Interestingly, during neuronal lesioning, the burst duration remains quite stable, with a mean spike frequency around 58.1 $\pm$ 2 Hz during burst.

The fraction of lesioned neurons leading to burst termination in our model is around 40%, whereas in [5], the estimated value coming from experiments was between 15 and 20 %, showing that our model is too robust. This robustness could result from the mean-field modeling used for the synaptic dynamics, which does not account for synaptic failures. To test this hypothesis, we modified this aspect of the model, by introducing a release probability parameter P_{rel} in the

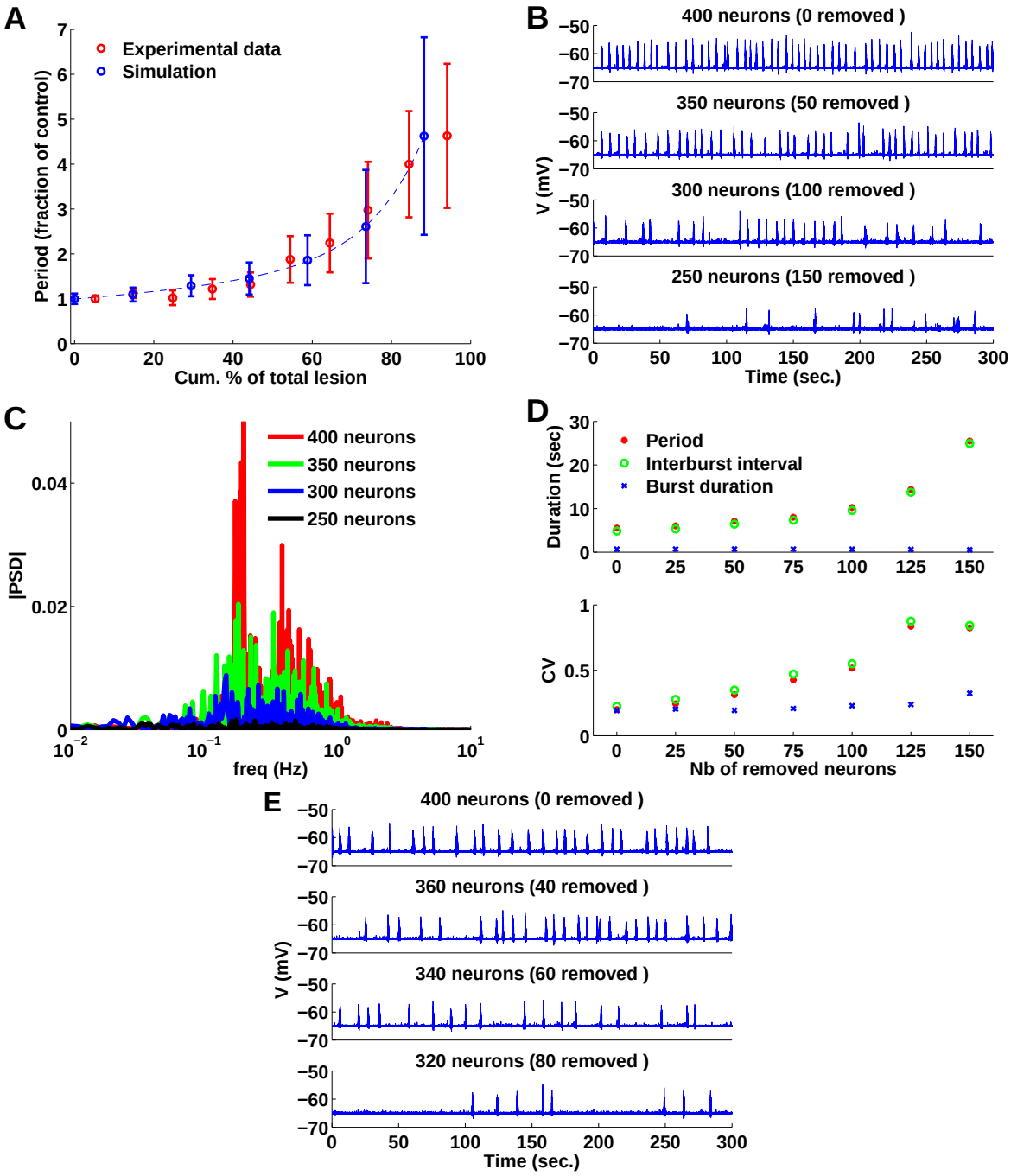

Figure S7: **Effect of deleting random neurons on the network activity.** **A**: Comparison between simulations (blue) and experimental results (red, extracted from [5]). **B**: Mean membrane potential when 0, 50, 100, and 125 neurons are removed, corresponding to 400, 350, 300 and 275 remaining neurons. **C**: Power spectrum associated with **B** (logarithmic scale). **D**: Mean and CV of the burst duration, interburst interval and rhythm period for several removed neurons. **E**: Mean membrane potential when 0, 40, 60, 80 neurons are removed in a network of 400 neurons, with a release probability P_{rel}=0.8.

system of eqs. 10 governing vesicular release:

$$\begin{aligned}
\dot{x} &= \frac{X-x}{\tau_f} + k(1-x)H(V-T) \\
\dot{y}_{\text{free}} &= \frac{1-y_{\text{free}}-y_{\text{dock}}}{\tau_{\text{rec}}} - \frac{1}{\tau_{\text{dock}}}\left(y_{\text{dock}}^{\max}-y_{\text{dock}}\right) y_{\text{free}} \left[1+\frac{x-X}{X}H(V-T)\right] \qquad (15) \\
\dot{y}_{\text{dock}} &= \frac{1}{\tau_{\text{dock}}}\left(y_{\text{dock}}^{\max}-y_{\text{dock}}\right) y_{\text{free}} \left[1+\frac{x-X}{X}H(V-T)\right] \\
&\quad -\frac{1}{\tau_{\text{rel}}} y_{\text{dock}} \frac{x-X}{X} H(V-T)H(r-P_{\text{rel}}),
\end{aligned}$$

where r is a uniform random variable on $[0,1]$. We used a value of this parameter P_{rel}=0.8. We simulated the network and we found the following changes: the cycle period is increased from 5.0 ± 1 to 9.8 ± 4.1 sec. When removing 80 neurons, we observe very few bursts with IBIs lasting more than 80 sec, and a clear disruption of the rhythm (Fig. S7**E**). We conclude that by introducing a stochastic release, our model can now replicate the disruption of the rhythm with a similar robustness as in lesioning experiments.

2.6 Consequences of gradually decreasing the synaptic strength. Fig. S8

To study the consequences of decreasing the synaptic strength, we decreased parameter K_I in the model, which has an effect equivalent to applying [NBQX], an antagonist of AMPARs that mediate synaptic transmission and underlie respiratory drive in the preBötzinger Complex [6]. We implemented the numerical procedure as follows: we chose a network with randomly connected neurons and ran simulations over 300 seconds while decreasing values of K_I, from 100% $K_I = 2666$ to 60% $K_I = 1600$ in steps of 2%. For values lower than 70%, we ran simulations for 900 seconds to account for a sufficient amount of periods. We observed a steep increase in the rhythm period, with no major changes in burst duration (Fig. S8). The rhythm started to be highly irregular at 68%, with interburst intervals lasting more than 100 seconds, and disappeared around 60%. The curve is well-fitted by a double exponential (dashed curve in Fig. S8A, SSE = 0.94). To compare with experimental data extracted from [6], we considered that the control conditions in simulations (100% control) corresponds to 0.001 μM [NBQX]. We then scaled the abscissa of the simulation plot so that the two curves best match (Fig. S8A).

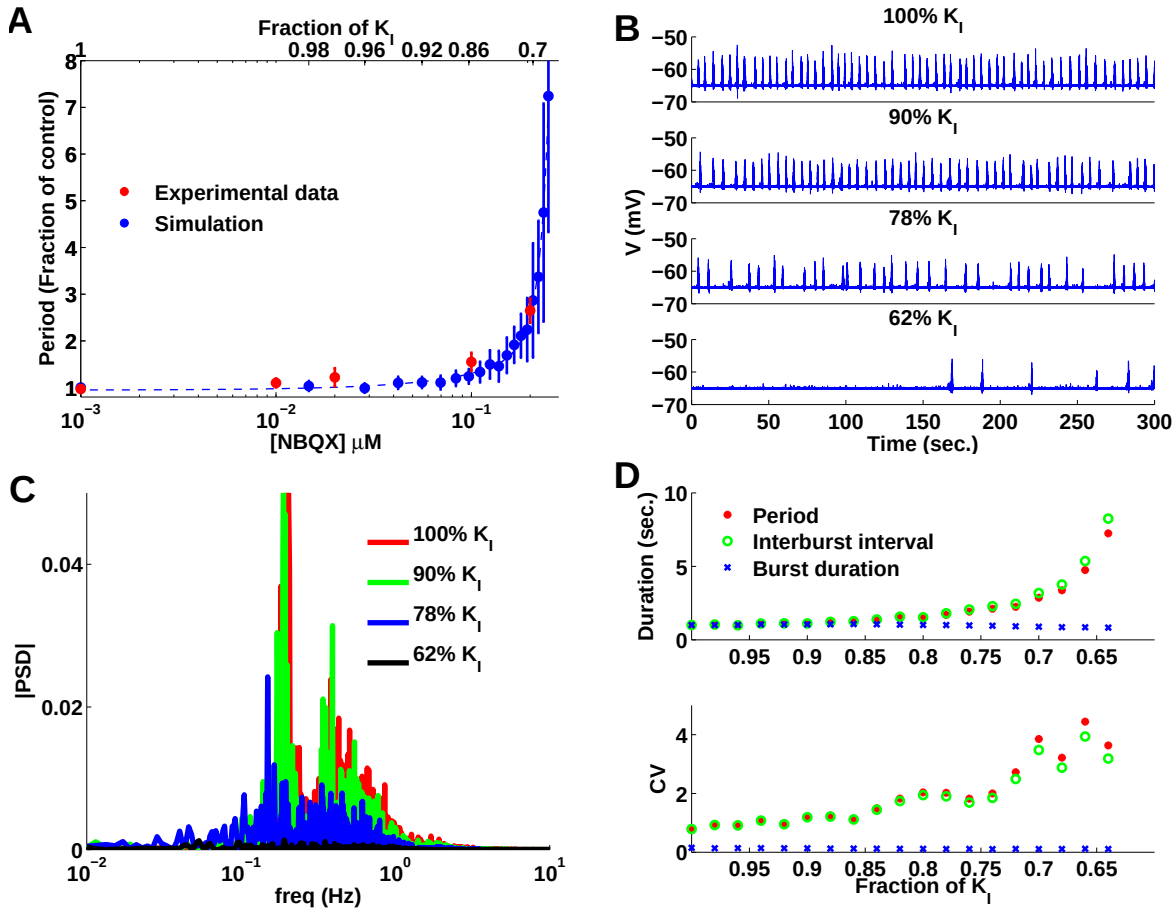

Figure S8: **Consequences of gradually decreasing synaptic strength, comparison with experimental data.** **A**: Comparison between simulations (blue) and experimental results (red, extracted from [6]). Results are presented as mean ± S.E.M. **B**: Mean potential over all the network for different values of the fraction of the initial synaptic strength, controlled via K_I. **C**: Power spectrum of the mean membrane potential computed for several fractions of K_I. **D**: Mean and CV of the burst duration, interburst interval, and rhythm period for several fractions of K_I.

2.7 Depolarizing neurons increases the rhythm frequency. Fig. S9-S10-S11

Changing (depolarizing and hyperpolarizing) the membrane potential affects bursting: to depolarize (hyperpolarize) neurons, we added (or subtracted) a current I_{app} to their current balance equation (Fig. S9). This current is equivalent to increasing the extracellular potassium concentration [K^+] and the probability of ectopic spikes. To compare experimental and simulation data, we scaled the abscissa and superimposed the two curves, where 9 mM [K^+] corresponds to control conditions ($I = 0$, no additional current).

At 9 mM [K+], the correspondence between preBötC and XIIn activity is known to be almost one-to-one [7], whereas at 6 mM and 3 mM [K^+], Kam et al [8] observed burstlets in the preBötC activity that do not show up in XIIn activity. Burstlets are characterized by smaller amplitude than preBötC bursts. In our model, for I_{app}=-0.25 pA and I_{app}=-0.5 pA, we observe periods of times during the interburst interval where several neurons are spiking together but no population-wide activity is generated (see the red line in Fig. S10**A**).

This effect recalls the pre-inspiratory patterns observed in control conditions (I_{app}=0 pA, green line in Fig. S10**A**): before each spike, a small group of tens of neurons, that differs from one burst to another, spike together, and recruit the entire network for a bursting event (see Supp Movie S3). Those neurons could represent the pre-inspiratory neurons observed experimentally. We postulate that after hyperpolarization of the network (I_{app}=-0.25 pA), those groups of neurons fail to recruit the entire network; likely because of the hyperpolarization that makes recruitment more difficult. These patterns, formed by small groups of tens of spiking neurons that do not trigger a burst, show similarities with the burstlets observed experimentally [8]. Nevertheless, burstlet activity observed in [8] is widespread in the preBötC and not restricted to a small number of neurons like in our model.

To investigate how hyperpolarization of the network modifies the rhythm's dynamics, we plotted Poincaré maps of the cycle periods when I_{app} = -0.25 pA over 1000 sec (Fig. S10**B**, nine runns). We observed a wide, quasi-periodic distribution comparable to the experimental results observed in ([8], Figure 1D), which was different from the single cluster expected when the system is regularly periodic (I_{app} = 0 pA, Fig. S10**C**). We conclude that hyperpolarization of the network modifies the rhythm's dynamics and an almost periodic regime appears as revealed by the Poincaré maps.

To clarify the mechanism of these low amplitude events (red in Fig. S10**A**) in our study, we now show using numerical simulations (Fig. S11) that contrary to the burst activity, which extends through the neuronal network, during these events, the synaptic properties (depression and facilitation) are not involved, preventing the recruitment of the network.

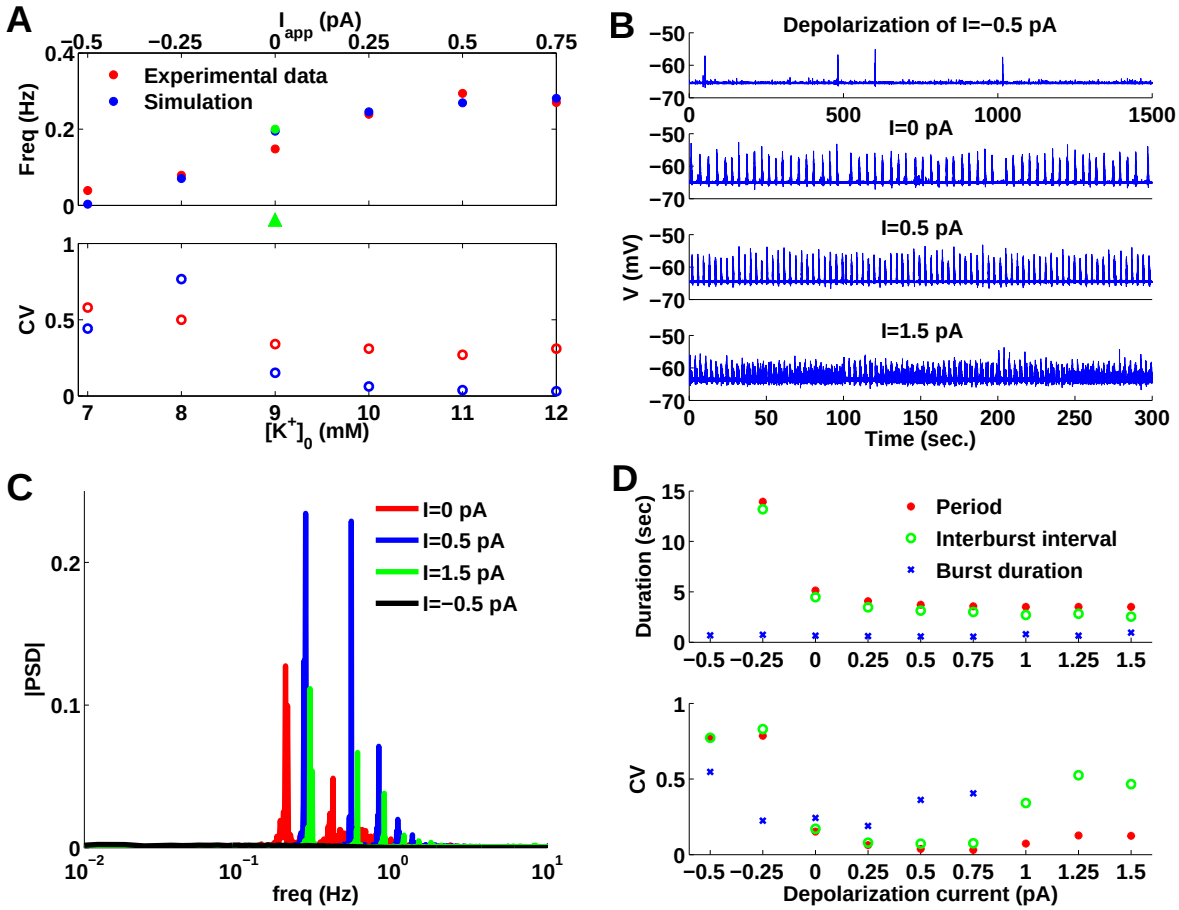

Figure S9: **Consequence of a global neuronal depolarization on the network rhythm.** **A**: Comparison between experimental results published in [7] (red) and simulations (blue). The experimental results are obtain by moving the extra-cellular potassium concentration from 3 mM to 12 mM. To compare with the simulations, we scaled the abscissa and superimposed the two curves, taking into account that 9 mM corresponds to control conditions. The green circle represents the mean frequency in control conditions (at 9 mM $[K^+]$, green arrowhead), which differs during the experimental protocol. **B**: Mean potential over all the network for different values of I. **C**: Power spectrum associated with **C**. **D**: Mean and CV of the burst duration, interburst duration and rhythm period for several values of the applied current I_{app}.

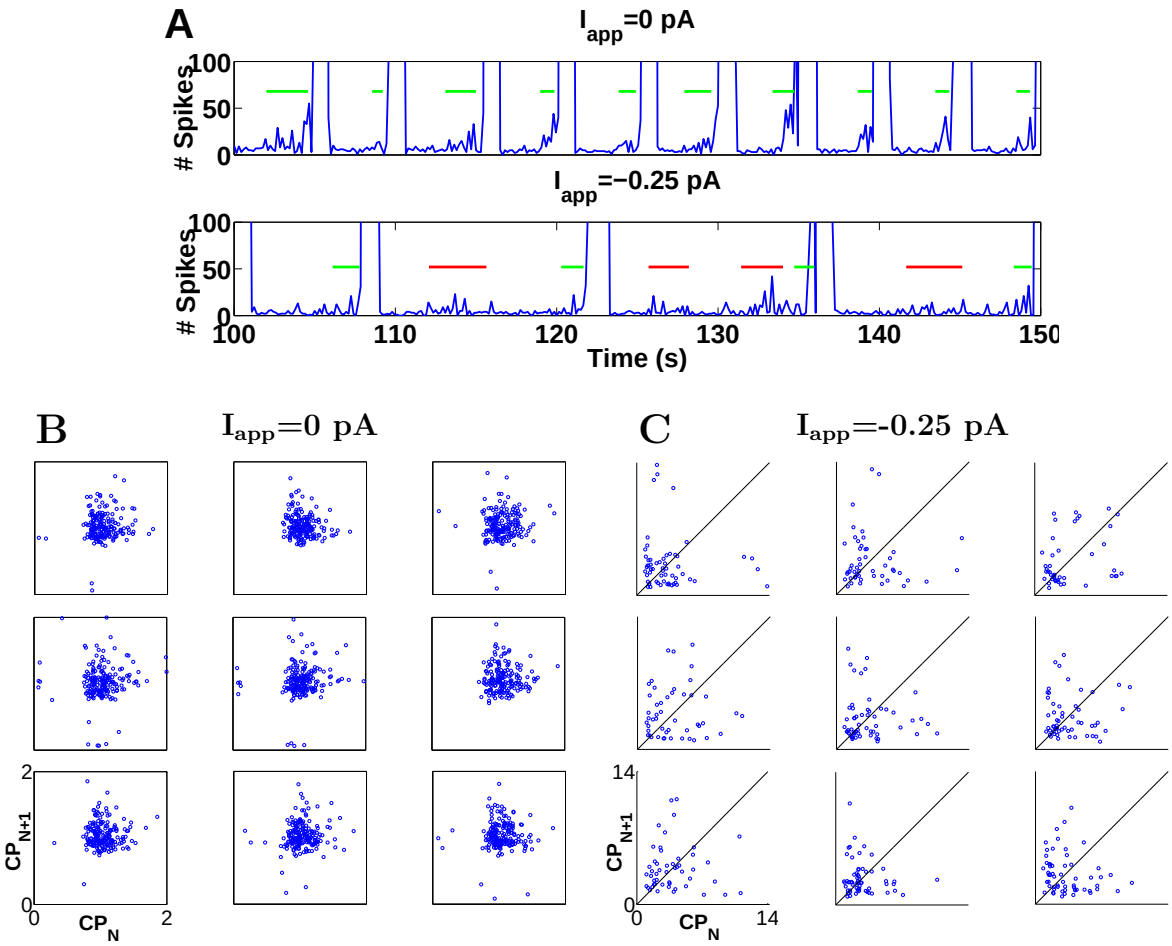

Figure S10: **Network-wide hyperpolarization A**: Time dependent plot of the number of spikes in the network when no current is applied (I_{app} = 0 pA, top), and when the network is hyperpolarized (I_{app} = -0.25 pA, bottom). Note the increasing spiking activity preceding the burst (green bars) in both plots. The red bars show periods when several neurons are spiking together but fail to recruit the network, which show similarities (but see text) with the burstlets observed experimentally. **B-C**: Poincaré maps of the cycle periods of one random neuron when I_{app} = 0 pA (**B**) and I_{app} =-0.25 pA (**C**). The network is recorded over 1000 sec (nine runs), cycle periods are normalized by the mean period when I_{app} = 0 pA, equal to 5.0 sec. Notice the difference in the axes range in **B** and **C**.

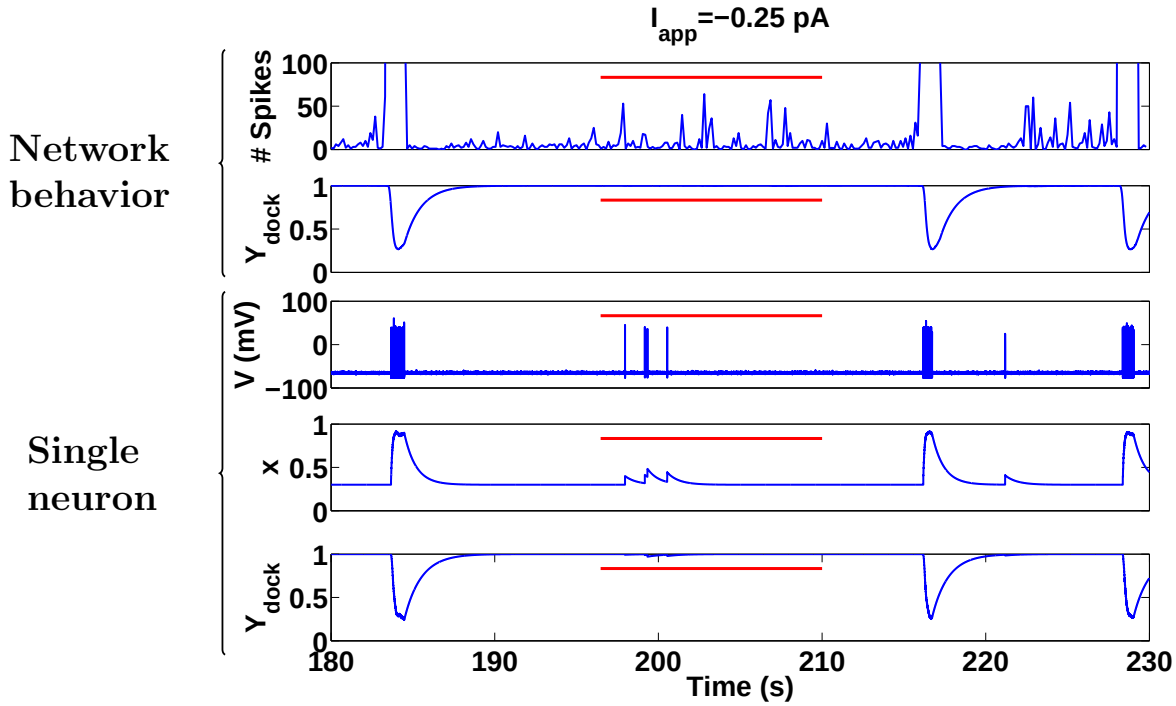

Figure S11: **Low amplitude events and synaptic properties.** Low amplitude events are observed when the network is hyperpolarized by I_{app}=-0.25 pA. Time dependent plot of the number of spikes in the network (first), the mean depression over the network $Y_{\text{dock}} = y_{\text{dock}}/y_{\text{dock}}^{\max}$ (second graph), the potential of a single neuron(third graph), the facilitation (fourth) and the depression variable Y_{dock} of a single neuron (last). Low amplitude activity events involving few neurons (red lines) cannot trigger a burst. During low amplitude events the depression and facilitation variables are not activated. Thus the synaptic properties are not involved in their termination, in contrast to bursts.

2.8 Minimal number of stimulations for burst induction.

To determine the minimal number of neurons necessary for inducing a network burst (Fig. 2D), we depolarized an increasing number of randomly chosen neurons. In practice, within the HH-model, we generated trains from 1 to 6 events consisting of 100 mV-depolarization during 0.05 ms with an interval separation of 17 ms between the train (at 60 Hz). This 60 Hz-frequency corresponds to the endogenous spiking dynamics. We started running the network at time $t = 0$ while we generated the stimulation at time t=550 ms, where steady state is achieved. We then monitored for 2 seconds the activity. A burst was detected when 80% of the neurons were spiking one second after initiation. We could then estimate the probability of bursting for different numbers of pulses and stimulated neurons.

2.9 Inspiratory drive currents. Fig. S12

Experimentally, respiratory preBötC neurons receive a volley of inward synaptic currents that typically last for hundreds of milliseconds, peak at more than 100 pA, occur at periodic intervals, and are referred to as inspiratory drive currents (Fig. S12).

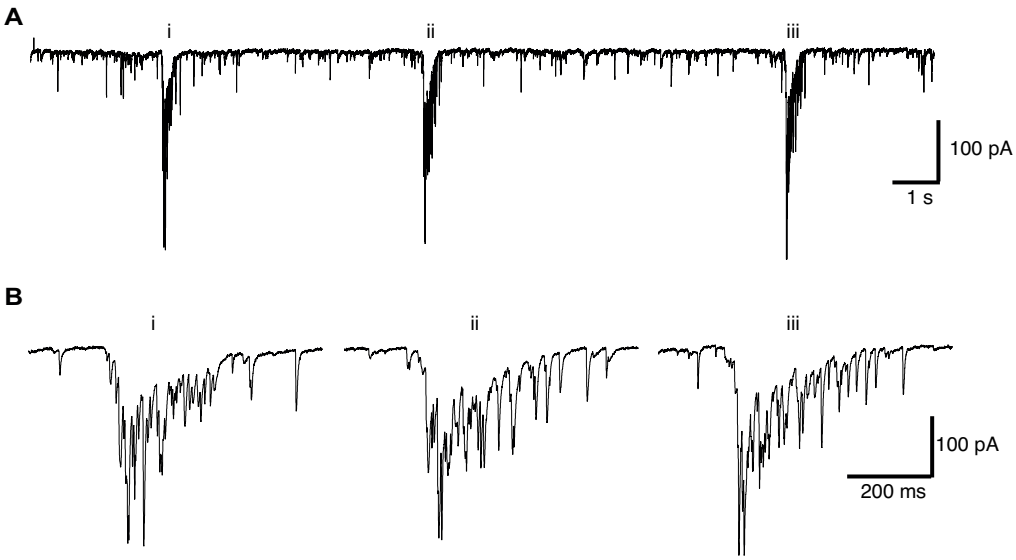

Figure S12: **Inspiratory drive currents in an experimentally-recorded preBötC neuron** **A**: Inspiratory drive currents in voltage-clamp configuration. The command voltage was -60 mV, and this is an expanded view of the trace displayed in the middle of Fig. 3C. **B**: Individual bursts (i., ii., iii.) are shown at a faster timescale.

Tables

Table 1: Parameters of synaptic transmission

Parameter	Description	Value
x	Facilitation variable	
y_{dock}	First depression variable	
y_{free}	Second depression variable	
X	Equilibrium value of x	0.3
x_{RefP}	Threshold for refractory period	0.31
$y_{\text{free}}^{\text{max}}$	Maximum value of y_{free}	0.82
$y_{\text{dock}}^{\text{max}}$	Maximum value of y_{dock}	0.18
$y_{\text{dock}}^{\text{min}}$	Minimum value of y_{dock}	0.04
k	Facilitation parameter	0.08
τ_f	Facilitation time constant	700 ms
τ_{dock}	First time constant for y_{dock}	738 ms
τ_{rel}	Second time constant for y_{dock}	47 ms
τ_{rec}	Time constant for the recovery	3000 ms
τ_{del}	Delay of the synaptic response	1 ms
K_I	Synaptic strength	2666
s	Connectivity	0.9
σ	Amplitude of voltage noise	0.89 $(\text{pA.cm}^{-2})^2.\text{ms}^{-1}$
T	Action Potential threshold	-58 mV

Table 2: Hodgkin-Huxley

Parameter	Description	Value
C	Capacitance	1 μF.cm^{-2}
g_{Na}	Conductance of Na^{2+}-current	120 mS.cm^{-2}
V_{Na}	Equilibrium potential of Na^{2+}-current	50 mV
τ_m	Parameter for m	10 ms
θ_m	Parameter for m	-40 mV
η_m	Parameter for m	4
σ_m	Parameter for m	18
g_K	Conductance of K^+-current	36 mS.cm^{-2}
V_K	Equilibrium potential of K^+-current	-77 mV
g_L	Conductance of leak current	0.3 mS.cm^{-2}
V_L	Equilibrium potential of leak current	-54.4 mV
τ_n	Parameter for n	100 ms
θ_n	Parameter for n	-55 mV
η_n	Parameter for n	0.125
σ_n	Parameter for n	80

References

[1] Ruangkittisakul A, Panaitescu B, Ballanyi K (2011) K^+ and Ca^{2+} dependence of inspiratory-related rhythm in novel calibrated mouse brainstem slices. *Respir Physiol Neurobiol* 175(1):37-48.

[2] Edelstein A, Amodaj N, Hoover K, Vale R, Stuurman N (2010) Computer control of microscopes using μManager. *Curr Protoc Mol Biol* 14.20.1-14.20.17.

[3] Tsodyks M, Pawelzik K, Markram H (1998) Neural Networks with Dynamic Synapses. *Neural Comput* 10(4):821-835.

[4] Bressloff PC, Coombes S (2000) Dynamics of strongly coupled spiking neurons. *Neural Comput* 12(1):91-129.

[5] Hayes JA, Wang X, Del Negro CA (2012) Cumulative lesioning of respiratory interneurons disrupts and precludes motor rhythms *in vitro*. *Proc Natl Acad Sci USA* 109(21):8286-8291.

[6] Morgado-Valle C, Feldman JL (2007) NMDA receptors in preBötzinger complex neurons can drive respiratory rhythm independent of AMPA receptors. *J Physiol* 582(1):359-368.

[7] Del Negro CA, Kam K, Hayes JA, Feldman JL (2009) Asymmetric control of inspiratory and expiratory phases by excitability in the respiratory network of neonatal mice *in vitro*. *J Physiol* 587(6):1217-1231.

[8] Kam K, Worrell JW, Janczewski WA, Cui Y, Feldman JL (2013) Distinct inspiratory rhythm and pattern generating mechanisms in the preBötzinger Complex. *J Neurosci* 33(22):9235-9245.